APPLIED PHYSICS

Voltage-driven, local, and efficient excitation of nitrogen-vacancy centers in diamond

**Dominic Labanowski[1,2]*, Vidya Praveen Bhallamudi[3]*†, Qiaochu Guo[3],
Carola M. Purser[3], Brendan A. McCullian[3], P. Chris Hammel[3], Sayeef Salahuddin[1]‡**

Magnetic sensing technology has found widespread application in a diverse set of industries including transportation, medicine, and resource exploration. These uses often require highly sensitive instruments to measure the extremely small magnetic fields involved, relying on difficult-to-integrate superconducting quantum interference devices and spin-exchange relaxation-free magnetometers. A potential alternative, nitrogen-vacancy (NV) centers in diamond, has shown great potential as a high-sensitivity and high-resolution magnetic sensor capable of operating in an unshielded, room-temperature environment. Transitioning NV center–based sensors into practical devices, however, is impeded by the need for high-power radio frequency (RF) excitation to manipulate them. We report an advance that combines two different physical phenomena to enable a highly efficient excitation of the NV centers: magnetoelastic drive of ferromagnetic resonance and NV-magnon coupling. Our work demonstrates a new pathway that combine acoustics and magnonics that enables highly energy-efficient and local excitation of NV centers without the need for any external RF excitation and, thus, could lead to completely integrated, on-chip, atomic sensors.

INTRODUCTION

Experiments investigating high-sensitivity magnetometry with nitrogen-vacancy (NV) centers commonly require the application of a microwave frequency excitation on the order of 1 to 10 W (1–3). The need for such large excitation power not only complicates the integration of the sensors in a small footprint but also has the potential to substantially perturb the environment that it is trying to measure. For example, a 10-W microwave excitation traveling in a standard 50-ohm stripline creates a magnetic field of approximately 90 µT at a distance of 1 mm, thus making it impossible to take advantage of the intrinsic ability of NV centers to detect fields on the order of tens of femtoteslas in an unshielded environment (4).

One potential mechanism for localizing the influence of the incident radio frequency (RF) power to the diamond NV centers is to leverage the recently observed interaction between NV centers in diamond and a proximal resonating ferromagnet (5–8). The time-varying excitations responsible for the NV–ferromagnetic resonance (FMR) coupling are spatially periodic magnons, whose magnetic effects should be entirely confined to within a few wavelengths (on the order of micrometers or less for these systems). Commonly, however, such systems run into the same problems of high-power RF excitation—with studies using more than 15 W of microwave power to obtain low-noise measurements (7, 8).

Here, we report an advance that combines two different physical phenomena to enable a highly efficient excitation of the NV centers (see Fig. 1). The energy flows in this combined system are outlined in Fig. 1C. The first of these is the recent demonstration that FMR in a thin ferromagnetic film can be excited using magnetoelastic

interaction with a piezoelectric material (9–12). This allows for the excitation of a purely voltage-driven FMR. The magnetoelastic interaction transduces acoustic excitations into an internal effective magnetic field within the ferromagnet. As a result, the field is extremely local and resides within the ferromagnetic film atop the piezoelectric material. In addition, this effective magnetic field is several orders of magnitude more efficient than traditional FMR excitation via Oersted fields in a stripline (12), reducing the input power requirement by the same amount. Once the ferromagnet is excited into FMR, the highly local interaction between the NV centers and spatially periodic magnons can now be used to excite the NV centers. This NV-magnon coupling is also extremely efficient, showing comparable Rabi frequencies to microwave excitation using over 1000 times more power (at an NV-antenna spacing of 20 µm) (13, 14). Therefore, the entire interaction from piezoelectric to NV centers is highly local and efficient. This combination of localized interaction and reduced input power requirements leads to minimal perturbation of the surrounding environment.

RESULTS

A schematic diagram of our experiment can be found in Fig. 1A, and an optical image of a measured device can be found in Fig. 1B. The system consists of an acoustically driven FMR (ADFMR) device where microfabricated resonant interdigitated transducers (IDTs) launch surface acoustic waves (SAWs) in the piezoelectric LiNbO$_3$ substrate when driven with a microwave voltage. A ferromagnetic pad, either cobalt or nickel (with a thickness of 20 nm), is located on top of the substrate. Nanodiamonds containing NV centers were deposited at multiple locations on top of the ferromagnetic pad to enable localized optical detection of the ADFMR. These spots can be seen as the dark circles in the optical image.

Figure 2 shows ADFMR absorption data collected from a 20-nm nickel device at 1429 MHz. The dependence of absorption on applied magnetic field and field angle can be seen in Fig. 2A. The characteristic fourfold symmetry evident in the angular scan is

[1]Department of Electrical Engineering and Computer Sciences, University of California, Berkeley, Berkeley, CA 94720, USA. [2]Intelligence Community Postdoctoral Research Fellowship Program, University of California, Berkeley, Berkeley, CA 94720, USA. [3]Department of Physics, The Ohio State University, Columbus, OH 43210, USA.
*These authors contributed equally to this work.
†Present address: Department of Physics, Indian Institute of Technology Madras, Chennai 600036, India.
‡Corresponding author. Email: sayeef@berkeley.edu
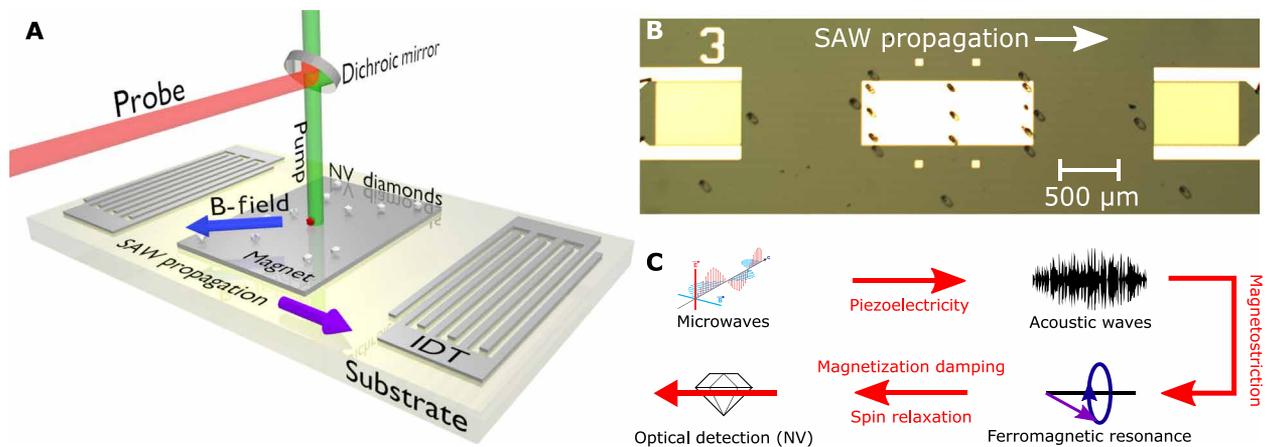
Fig. 1. Measured NV-ADFMR system. (**A**) Schematic diagram of the experimental sample and the optical excitation/detection scheme. The magnetic field was applied at 45° in-plane from the SAW propagation direction for all optically detected measurements to maximize the power absorption in the magnetic films due to ADFMR. Small particles on the magnetic pad indicate deposited nanodiamonds. (**B**) Photograph of measured device shows IDTs and the magnetoelastic film and indicates the direction of SAW propagation. Dark spots on the film and substrate are clusters of nanodiamonds. (**C**) Diagram of energy flow in the system, showing transduction methods between the different components of the sample. Microwave electrical energy is converted into acoustic energy via piezoelectricity, which then drives magnetic precession. As this precession damps, it generates magnons that couple to the NV centers, modulating their photoluminescence (PL).
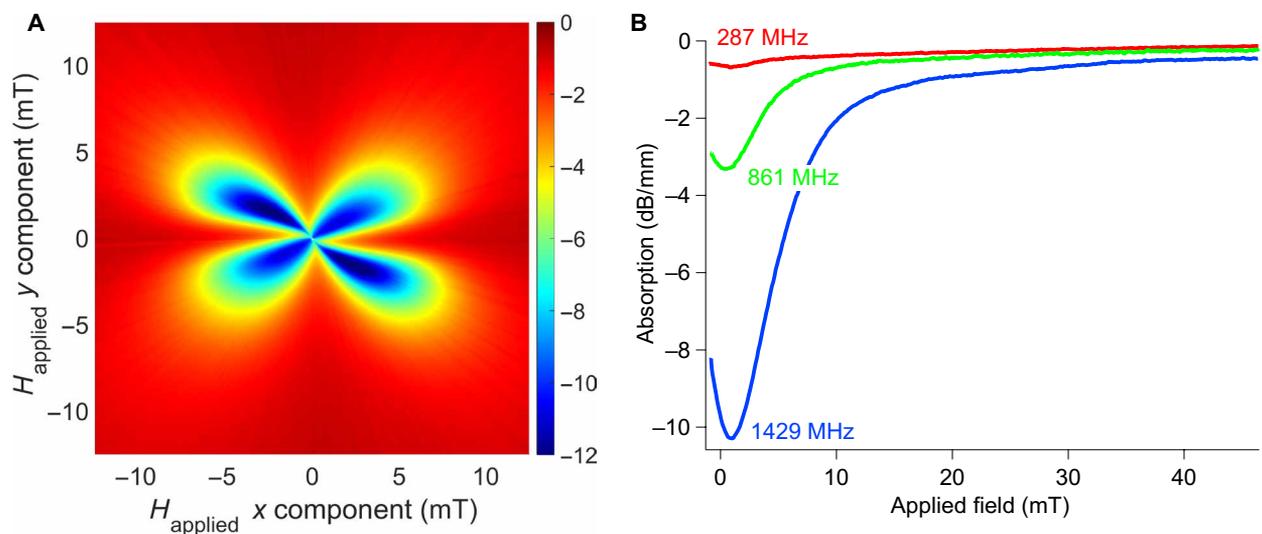
Fig. 2. Power absorption in ADFMR. (**A**) Plot of power absorption as a function of applied magnetic field for a 20-nm nickel ADFMR device at 1429 MHz. The x component of the field is taken to be parallel to the direction of SAW propagation, and the y component is in-plane and perpendicular to the direction of SAW propagation. The color bar indicates absorption in decibels per millimeter. (**B**) Line cut along the angle of highest absorption (45°) showing a large field-dependent attenuation at 287, 861, and 1429 MHz. Although absorption at 287 MHz appears small on a logarithmic scale compared to the other frequencies, absorption in a 1-mm film is still >0.69 dB or ≈15% at 287 MHz.

a direct consequence of the magnetoelastic driving field that excites ADFMR. An analysis of the magnetoelastic interaction between a ferromagnetic film and longitudinal SAWs shows that the amplitude of the effective magnetic field generated by this interaction varies as $\cos(\theta)\sin(\theta)$ (where θ is the angle between the magnetization and the direction of SAW propagation) (*15*). As the magnetic power absorption in ferromagnetic resonance varies directly with the square of the driving field, this dependence is clearly reflected in the power absorption spectrum.

Figure 2B shows a line cut of the field dependence along the angle of highest absorption (45°) from the SAW propagation

direction for all frequencies of excitation used in this study (287, 861, and 1429 MHz). The microwave absorption can be observed as extremely large for such a low-frequency excitation—several orders of magnitude more than a traditional stripline FMR excitation (*16*).

The ADFMR phenomenon occurs as a result of a combination of piezoelectric and magnetoelastic interactions. An RF voltage applied to an IDT first generates SAWs. These waves generate a time-varying strain that can alter the magnetocrystalline anisotropy of a magnetoelastic ferromagnet via the Villari effect and generate an effective magnetic field internal to the magnet (*10*). The

amplitude of this effective field as a function of applied strain and magnetoelastic coefficients has been previously derived by analyzing the free energy of the magnet in the presence of periodic elastic excitation (*15*). This effective field is capable of driving the system into FMR.

As the precession generated by ADFMR is damped, it emits spin waves over a range of frequencies (*7*). The NV center is a spin 1 defect whose PL is dependent on its spin state and is hyperpolarized into its 0 state by the 532-nm pump laser (*17*). The incoherent spin waves emitted by the precession as it damps can be resonant with the NV, causing the NV spins to relax. NV PL intensity is spin-dependent, being high for the 0 state and low for the ±1 state. Thus, as the NV spins relax because of FMR, their PL intensity changes and this change can be recorded.

Figure 3A shows the change in NV center PL under different conditions for a nickel device. The frequency sweeps done around the first, third, and fifth harmonics (287, 861, and 1429 MHz, respectively) of the IDTs are shown; the IDTs only allow odd harmonics to be transmitted as they are patterned with a 50% metallization ratio (*18*). The scans shown in Fig. 3A are representative scans to demonstrate the optical detection of ADFMR. The amplitude of the peaks can vary between samples and between nanodiamond clumps on the same sample, in addition to the variation due to position and frequency. Near the edge of the ferromagnetic pad closest to the excitation IDT, at higher frequencies, the average fractional change is approximately 1%, which is comparable to the signal observed in other NV-FMR coupling experiments using diamond nanocrystals (*5*). All data for PL change presented in this paper are fractional change, that is, lock-in voltage/DC voltage.

Clear peaks in the optical signal can be seen for nanodiamonds at zero magnetic field and on the nickel pad (blue). The NV spins by themselves should not have any signal at 287 and 861 MHz since they are far away from any NV resonances in zero field. However, at 1429 MHz, a direct drive signal can be observed since this coincides closely with the NV's excited state resonance frequency. To check the origin of the signal, we performed a control measurement away from the ferromagnetic pad (red), which shows no signal even at 1429 MHz, although this spot was closer to the input IDT and should have a larger amplitude of acoustic waves (and spurious microwaves). Thus, we can rule out any spurious interaction of the acoustic waves or microwaves directly with the NV in our experiment. Although strain waves can couple to the NV center (*19*, *20*), we do not see any evidence for this interaction in our experiment—most likely because of the very weak mechanical coupling between the substrate and the nanodiamonds. To further verify the FMR origin of the peaks scene in the blue data, we measured the signal at a higher field (green). A field strength of 35.8 mT is sufficient to bias the magnetic films out of resonance. As it can be seen, we observe no PL signal at these fields. Thus, our control measurements verify that the peaks scene in the blue data is due to FMR.

Next, we demonstrate the local nature of the drive by recording spatially localized data across the ADFMR device. Figure 3B shows the change in fractional NV PL at zero field for the 20-nm nickel device as a function of longitudinal position, that is, distance from the edge of the nickel pad closest to the excitation IDT along the SAW propagation direction. The data presented here are an average of three spots that are the same distance from the edge of the nickel pad (see inset). This averaging helps mitigate the effect of inhomogeneity in nanodiamond spots at various locations. The distance between the NV centers and the ferromagnet determines coupling efficiency, and thus, inhomogeneity arising from the deposition process can lead to a noisy signal.

These direct spatial measurements performed via coupling to NV centers provide another means of measuring the power absorption data shown in Fig. 2B. At 287 MHz, the PL amplitude is constant (within measurement error) over the full length of the film, as would
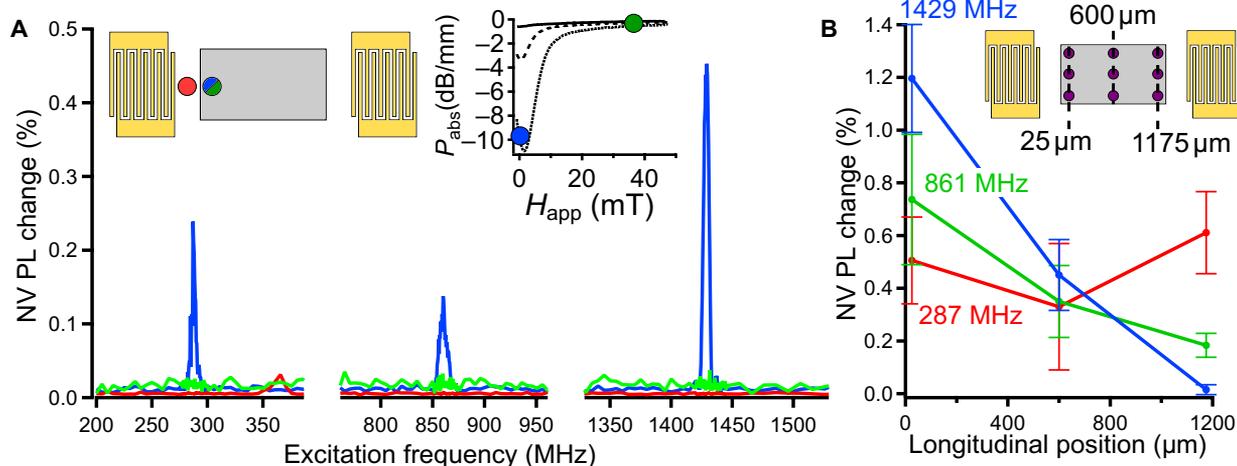
Fig. 3. Frequency and spatial dependence of NV-ADFMR coupling in nickel devices. (**A**) Change in NV center PL normalized to the DC level for nanodiamonds both on and off the ferromagnetic pad. NV centers located off the ferromagnetic pad (red) and NV centers on the pad with a high (35.8 mT) applied bias field (green) show no change in PL. Only NV centers on the pad with zero applied bias field (blue) show a notable PL change. All measured NV PL change outside the shown frequency range is within noise. (Inset) Left: Position of the NV centers on the device. Right: Power absorption of the ferromagnetic film along the applied field direction at the field values of interest. The colors in the insets correspond to the colors in the figure. The peaks in the NV center signal align with the first, third, and fifth harmonics of the IDTs. (**B**) NV PL change in a 20-nm nickel sample as a function of longitudinal position from the edge of the ferromagnet closest to the excitation IDT. Measurements were performed with the drive frequency set to the first (red), third (green), and fifth (blue) harmonics of the IDTs and at zero applied magnetic field. (Inset) Schematic illustration of nanodiamond positions.
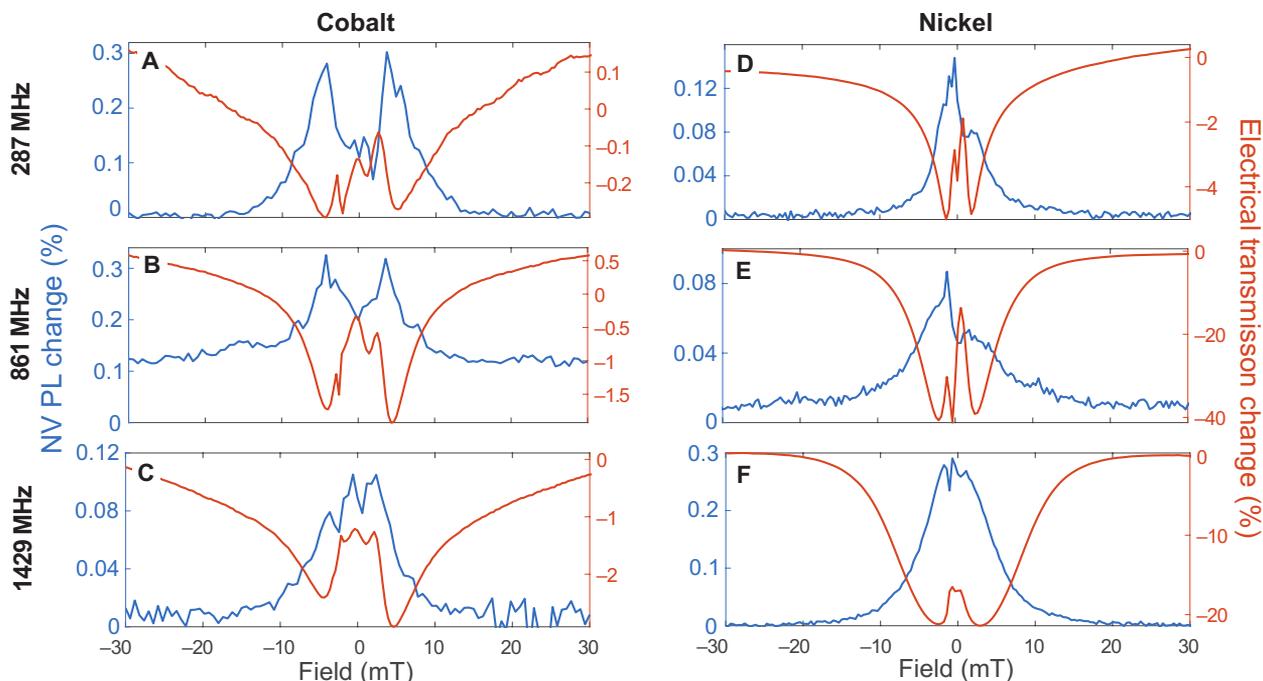
Fig. 4. Magnetic field dependence of NV-ADFMR coupling. Microwave power absorption and NV PL change as a function of magnetic field in nickel and cobalt samples. The drive frequency for the ADFMR devices was set to the first, third, and fifth harmonics of the IDTs for these measurements. A clear correlation between power absorption (right axis, red) and NV PL change (left axis, blue) can be observed.

be expected given the relatively small power absorption seen at this low frequency. As the excitation frequency is increased, the NV PL change can be seen to decrease as a function of distance from the leading edge of the film. This decrease is due to absorption of the excitation signal as it travels through the magnetic layer. These measurements corroborate previous measurements of ADFMR power absorption as a function of magnetic element length (*11*) and excitation frequency (*10*, *11*, *21*).

We now provide further evidence for optical detection of ADFMR by performing field sweeps around these IDT harmonic frequencies for both cobalt and nickel devices. These data are presented in Fig. 4, where we show change in the detected electrical signal (corresponding to absorption in the ferromagnetic film) in addition to the optical signal. The correlation between the optical signal and the transmission signal can be seen, especially in the case of cobalt. No peaks in the optical signal were seen in nanodiamonds not located on the ferromagnetic pads. It should be noted that, although we have previously detected FMR in cobalt using our relaxation-based technique, this is the first report of optical detection of FMR in nickel using NV centers. The peak heights of the optical signal are comparable in both cobalt and nickel, although the absorption signal is an order of magnitude (or more) larger in nickel films. This would imply that the coupling between nickel and NV centers is much smaller than for the case of cobalt. The reason for dependence of the coupling on the magnetic material is currently unknown.

DISCUSSION
Efficacy of the microwave versus acoustic drive for manipulating the NVs can be analyzed by comparing the amplitude of NV PL change for a given excitation power at the NV center. Compared to previous

work on NV-FMR coupling that directly used microwaves instead of acoustic waves (*5*), we find that similar NV PL change can be observed with 1300 times less power at the NV center location for an excitation frequency of 1429 MHz. Not unsurprisingly, we find the acoustic drive to be most efficient with the frequency that coincides with the NV's excited state resonance. This overlap with intrinsic resonances of the NV centers also opens possibilities of highly efficient coherent coupling to the 2.87-GHz ground state of the NV center with improved SAW devices. Even for the 287- and 861-MHz peaks, we find smaller but still orders of magnitude improvement with the acoustic drive compared to the direct microwave drive. Further details of this efficiency comparison can be found in the Supplementary Materials.

To summarize, we demonstrate a new pathway for off-resonant excitation of NV centers in diamond. A voltage-driven acoustic wave can generate FMR in a ferromagnetic thin film by exploiting magnetostriction. This FMR in turn couples with NV centers through spatially varying magnons. Both the SAW-FMR and FMR-NV coupling mechanisms are highly local. In addition, the magnetostriction-driven FMR is a few orders of magnitude more efficient as compared to conventional Oersted field–driven FMR (*12*). Given optimized IDT designs that do not suffer from large insertion losses, it should be possible to drive such a coupled system at extremely low power levels—reducing input power requirements by three orders of magnitude (from more than 1 W to the submilliwatt range). Thus, the combination of acoustics-to-magnonics-to-NV centers allows for an extremely local and energy-efficient way to excite the NV centers without perturbing the surrounding environment. Although we have used PL to probe the NV centers in this first demonstration, it is conceivable that, with proper optimization, it should be possible to detect them purely electrically by observing the power absorption

itself. The choice of atomic levels is also not limited to NV centers—any other defect center with zero field splitting should show similar behavior. Further work should focus on these possibilities, as well as the fundamentals of the coupling mechanism between the ferromagnet and the NV centers. Advances in these areas should lead to completely integrated, that is, both electrically driven and interrogated, atomic sensors that work close to their intrinsic limits.

MATERIALS AND METHODS
Device fabrication
ADFMR devices were fabricated on commercially available Y-cut LiNbO$_3$ wafers (MTI Corp) via standard I-line photolithography. IDT patterning was first performed on 4″ wafers using a GCA 8500 wafer stepper. After development, a low-power oxygen plasma treatment was performed using a Technics C Plasma Etching System to remove the remaining photoresist in the developed regions. Al contacts (100 nm) were deposited using a Technical Engineering Services thermal evaporator. The wafers were then diced into 8 mm × 8 mm chips using a Disco DAD3240 dicing saw, and second-layer photolithography with alignment was performed using a Canon 4X projection mask aligner. Following a second low-power oxygen plasma treatment, the nickel and cobalt films were deposited using a custom AJA e-beam evaporator and a custom AJA sputtering system, respectively. Commercial nano-diamonds containing NV centers (Adamas Nanotechnologies) were deposited by hand using laser-pulled glass pipettes at multiple locations on top of the ferromagnetic pad.

Electrical measurements
The angularly resolved power absorption measurements shown in Fig. 2 were performed using a custom-built setup that allowed for RF transmission measurements of a sample as it was rotated in relation to a fixed electromagnet (*12*). A signal generator was used to output an RF wave tuned to the first, third, and fifth harmonics of the IDTs (287, 861, and 1429 MHz, respectively), and a spectrum analyzer was used to measure the resulting output from the devices. Data shown in the figure were normalized to the transmitted power in the presence of a large (150 mT) applied field to remove the variation in device insertion loss when operating at different frequencies (*12*).

Because of the harmonic operation of the IDTs, device efficiency was dramatically reduced at higher operating frequencies. As a result of this low efficiency, the electromagnetic wave generated by the IDTs became comparable in amplitude to the acoustic signal at high harmonics. To obtain an accurate measurement of the magneto-elastic portion of the interaction, we leveraged the difference in wave speeds between acoustic and electromagnetic waves. Since acoustic waves travel ~100,000 times slower than electromagnetic waves, the two signals can be differentiated by using a time-gating technique (*9*, *11*, *12*, *22*).

The signal generator output was turned on for 700 ns and then turned off for 1300 ns (generating a 700-ns pulse with a period of 2 μs). Given the distance between the transducers and the speed of sound in the substrate, the acoustic propagation time was estimated to be approximately 800 ns. Thus, by only sampling the output signal after 800 ns had passed from the start of the pulse, it was ensured that only the acoustic component of the transmitted signal was being measured.

The electrical transmission data shown in Fig. 4 were obtained differently to allow for simultaneous measurement with the continuous-wave (CW) NV optical measurements. A +18-dBm microwave signal was modulated at low frequency and applied to the ADFMR devices. The output signal was routed to a Krytar 303BK power diode, whose output was connected to a lock-in amplifier tuned to the low-frequency modulation of the RF source. Because of the CW nature of the RF excitation, it was impossible to differentiate between the acoustic and electromagnetic waves. This explains the discrepancy between the power absorption shown at 1429 MHz in Figs. 2 and 4, as the data in Fig. 4 have an offset from the contribution of the electromagnetic wave (that is, not strongly modulated by the ferromagnetic film).

Optical measurements
Optical PL measurements were performed using two custom-built NV characterization setups. A 532-nm laser was used to excite the NV centers, and the resulting PL was measured using a photodiode in both cases. A lock-in measurement was performed by modulating the amplitude of the acoustic waves to enable the measurement of small changes in the NV PL. All optical measurements in this work were performed with the external bias field oriented at 45° in-plane from the SAW propagation direction to maximize the coupling between the applied acoustic excitation and the ferromagnetic films.

Measurements of NV PL were made with two similar pump-probe setups to collect data for this paper. Data in Figs. 3A and 4 were collected with one setup, and data in Fig. 3B were collected with another. Data from the setup used to collect data from Fig. 3B were used for efficiency calculations owing to a better understanding of RF loss in the system. Additional measurements from this setup can be found in the Supplementary Materials, showing a qualitative agreement with the data presented in Fig. 3A.

SUPPLEMENTARY MATERIALS
Supplementary material for this article is available at http://advances.sciencemag.org/cgi/content/full/4/9/eaat6574/DC1

Section S1. Comparison of power efficiency between NV-FMR and NV-ADFMR couplings
Section S2. Calculation of power at the magnetic element
Section S3. Comparison of measurement setups
Fig. S1. NV PL change as a function of RF power at the NV center location.
Fig. S2. NV PL change as a function of frequency for the two measurement setups used in this work.
Reference (*23*)

REFERENCES AND NOTES
1. C. C. A. Teale, "Magnetometry with ensembles of nitrogen vacancy centers in bulk diamond," thesis, Massachusetts Institute of Technology (2015).
2. H. Clevenson, M. E. Trusheim, C. Teale, T. Schröder, D. Braje, D. Englund, Broadband magnetometry and temperature sensing with a light-trapping diamond waveguide. *Nat. Phys.* **11**, 393–397 (2015).
3. A. Brenneis, L. Gaudreau, M. Seifert, H. Karl, M. S. Brandt, H. Huebl, J. A. Garrido, F. H. Koppens, A. W. Holleitner, Ultrafast electronic readout of diamond nitrogen-vacancy centres coupled to graphene. *Nat. Nanotechnol.* **10**, 135–139 (2015).
4. T. Wolf, P. Neumann, K. Nakamura, H. Sumiya, T. Ohshima, J. Isoya, J. Wrachtrup, Subpicotesla diamond magnetometry. *Phys. Rev. X* **5**, 041001 (2015).
5. C. S. Wolfe, V. P. Bhallamudi, H. L. Wang, C. H. Du, S. Manuilov, R. M. Teeling-Smith, A. J. Berger, R. Adur, F. Y. Yang, P. C. Hammel, Off-resonant manipulation of spins in diamond via precessing magnetization of a proximal ferromagnet. *Phys. Rev. B* **89**, 180406 (2014).
6. C. S. Wolfe, S. A. Manuilov, C. M. Purser, R. Teeling-Smith, C. Dubs, P. C. Hammel, V. P. Bhallamudi, Spatially resolved detection of complex ferromagnetic dynamics using optically detected nitrogen-vacancy spins. *Appl. Phys. Lett.* **108**, 232409 (2016).

7. C. Du, T. van der Sar, T. X. Zhou, P. Upadhyaya, F. Casola, H. Zhang, M. C. Onbasli, C. A. Ross, R. L. Walsworth, Y. Tserkovnyak, Control and local measurement of the spin chemical potential in a magnetic insulator. *Science* **357**, 195–198 (2017).

8. T. van der Sar, F. Casola, R. Walsworth, A. Yacoby, Nanometre-scale probing of spin waves using single electron spins. *Nat. Commun.* **6**, 7886 (2015).

9. M. Weiler, L. Dreher, C. Heeg, H. Huebl, R. Gross, M. S. Brandt, S. T. B. Goennenwein, Elastically driven ferromagnetic resonance in nickel thin films. *Phys. Rev. Lett.* **106**, 117601 (2011).

10. P. G. Gowtham, T. Moriyama, D. C. Ralph, R. A. Buhrman, Traveling surface spin-wave resonance spectroscopy using surface acoustic waves. *J. Appl. Phys.* **118**, 233910 (2015).

11. D. Labanowski, A. Jung, S. Salahuddin, Power absorption in acoustically driven ferromagnetic resonance. *Appl. Phys. Lett.* **108**, 022905 (2016).

12. D. Labanowski, A. Jung, S. Salahuddin, Effect of magnetoelastic film thickness on power absorption in acoustically driven ferromagnetic resonance. *Appl. Phys. Lett.* **111**, 102904 (2017).

13. D. Kikuchi, D. Prananto, K. Hayashi, A. Laraoui, N. Mizuochi, M. Hatano, E. Saitoh, Y. Kim, C. A. Meriles, T. An, Long-distance excitation of nitrogen-vacancy centers in diamond via surface spin waves. *Appl. Phys. Express* **10**, 103004 (2017).

14. P. Andrich, C. F. de las Casas, X. Liu, H. L. Bretscher, J. R. Berman, F. J. Heremans, P. F. Nealey, D. D. Awschalom, Long-range spin wave mediated control of defect qubits in nanodiamonds. *npj Quantum Inf.* **3**, 28 (2017).

15. L. Dreher, M. Weiler, M. Pernpeintner, H. Huebl, R. Gross, M. S. Brandt, S. T. B. Goennenwein, Surface acoustic wave driven ferromagnetic resonance in nickel thin films: Theory and experiment. *Phys. Rev. B* **86**, 134415 (2012).

16. I. S. Maksymov, M. Kostylev, Broadband stripline ferromagnetic resonance spectroscopy of ferromagnetic films, multilayers and nanostructures. *Physica E Low Dimens. Syst. Nanostruct.* **69**, 253–293 (2015).

17. J. Harrison, M. Sellars, N. B. Manson, Measurement of the optically induced spin polarisation of N-V centres in diamond. *Diamond Relat. Mater.* **15**, 586–588 (2006).

18. D. Morgan, Surface-wave devices for signal processing, in *Studies in Electrical and Electronic Engineering* (North Holland, 1991), vol. 19.

19. E. R. MacQuarrie, T. A. Gosavi, N. R. Jungwirth, S. A. Bhave, G. D. Fuchs, Mechanical spin control of nitrogen-vacancy centers in diamond. *Phys. Rev. Lett.* **111**, 227602 (2013).

20. D. A. Golter, T. Oo, M. Amezcua, K. A. Stewart, H. Wang, Optomechanical quantum control of a nitrogen-vacancy center in diamond. *Phys. Rev. Lett.* **116**, 143602 (2016).

21. M. Weiler, H. Huebl, F. S. Goerg, F. D. Czeschka, R. Gross, S. T. B. Goennenwein, Spin pumping with coherent elastic waves. *Phys. Rev. Lett.* **108**, 176601 (2012).

22. C. Deger, E. Born, H. Angerer, O. Ambacher, M. Stutzmann, J. Hornsteiner, E. Riha, G. Fischerauer, Sound velocity of $Al_x Ga_{1-x}$ N thin films obtained by surface acoustic-wave measurements. *Appl. Phys. Lett.* **72**, 2400–2402 (1998).

23. A. J. Slobodnik Jr., P. H. Carr, A. J. Budreau, Microwave frequency acoustic surface-wave loss mechanisms on $LiNbO_3$. *J. Appl. Phys.* **41**, 4380–4387 (1970).

Science Advances

Voltage-driven, local, and efficient excitation of nitrogen-vacancy centers in diamond

Dominic Labanowski, Vidya Praveen Bhallamudi, Qiaochu Guo, Carola M. Purser, Brendan A. McCullian, P. Chris Hammel and Sayeef Salahuddin

ARTICLE TOOLS	http://advances.sciencemag.org/content/4/9/eaat6574
SUPPLEMENTARY MATERIALS	http://advances.sciencemag.org/content/suppl/2018/08/31/4.9.eaat6574.DC1
REFERENCES	This article cites 21 articles, 1 of which you can access for free http://advances.sciencemag.org/content/4/9/eaat6574#BIBL
PERMISSIONS	http://www.sciencemag.org/help/reprints-and-permissions

Use of this article is subject to the Terms of Service